The influence of the vertical component of ground motion on the probabilistic treatment of the rocking response of free-standing blocks

Christos G. Lachanas,[1*] Dimitrios Vamvatsikos,[1] Michalis F. Vassiliou[2]

[1] School of Civil Engineering, National Technical University of Athens, Athens, Greece.
[2] Chair of Seismic Design and Analysis, DBAUG, ETH Zurich, Zurich, Switzerland.

Summary

The influence of the vertical component of ground motion is investigated for assessing the distribution of the seismic response of unanchored rigid blocks. Multiple stripes of site-hazard-consistent ground motions are employed for calculating the seismic response of rigid rocking blocks with and without the inclusion of the vertical component. The comparison of the resulting response is being made both for single records and full suites, employing a paired-record versus an ensemble-statistics comparison, respectively. It is shown that on a single record basis, the vertical component may have a non-negligible but highly variable influence on the rocking response, sometimes detrimental, sometimes beneficial. Still, when considering any large ensemble of records, the effect becomes statistically insignificant, except for the very specific case of rocking uplift for stocky blocks. To this end, for cases where the appearance of uplift is associated with damage, closed-form expressions are proposed to modify the lognormal fragility function of rocking initiation given the block slenderness and the ratio of the peak vertical over the peak horizontal ground acceleration.

KEYWORDS

rigid rocking blocks, multi-stripe analysis, seismic demands, vertical component, response statistics

1   INTRODUCTION

Since Housner's pioneer study in 1963 [1], the dynamics of the rocking response of unanchored rigid blocks have been the subject of numerous studies, [e.g., 2–13]. This interest stems from the application of the rocking oscillator as the seismic response mechanism in various structural types such as masonry structures [e.g., 14, 15], monumental structures [e.g., 16, 17], bridges [e.g., 18, 19], or building unanchored contents [e.g., 20, 21]. Most of the studies in the field have investigated thoroughly the response of the rocking oscillator under horizontal excitations. Both analytical pulses and earthquake ground motion waveforms, natural or artificial, have been studied, identifying the parameters that define the problem (block geometry and excitation characteristics).

Although most of the studies on the rocking block consider only the horizontal component of the excitation, there is also literature on the influence of the vertical component on rocking. For instance, Yim et al. [2], found that the vertical acceleration may significantly influence the rocking response. In a same pattern, Dimentberg [22] demonstrated that a strong vertical component, compared to the horizontal one, affects the overturning probability. Taniguchi [23] concluded that the vertical component should be included into the analysis of the seismic response of a rigid body since it adds irregularities on the different types of response. For instance, when slipping of the body is taken into account, the inclusion of the vertical acceleration helps the "liftoff-slip" interaction motion by reducing the friction between the block and its support base [23]. On the contrary, Ishiyama in 1982 [3], Shi et al. in 1996 [24], Makris and Zhang in 1999 [25], and recently Makris and Kampas [26] and Linde et al. [27] concluded that the vertical component has a negligible impact on the rocking response of slender blocks or even on the stocky ones for practical purposes. The main reasons for this marginal effect are the geometry of the problem, the typical low ratio of the vertical to horizontal component maximum acceleration, and the high-frequency content of the vertical component.

While some early concepts of probabilistic treatment of the problem at hand have appeared in the literature (especially [2,22]), they are naturally limited by the analysis capabilities of their era. Linde et al. [27] offer a more modern view, but mainly focusing on other salient aspects of the problem at hand. Herein, we attempt to comprehensively quantify the impact of the vertical component when the seismic response of rocking blocks is investigated within a state-of-art probabilistic framework for seismic vulnerability assessment. To this end, a comparative study is presented for the seismic response of rocking blocks with and without the inclusion of the vertical component of natural ground motions. Multi-Stripe Analysis (MSA) [28] is employed by using natural ground motions that have been selected to be consistent with site-specific seismic hazard via Conditional Spectrum (CS) techniques [29, 30, 31]. After the analysis, we present a direct comparison of the seismic response with and

---

[*] Corresponding author: lahanasch@central.ntua.gr

without the vertical component both on the basis of single records and entire ground motion suites, comparing both raw response and fragility functions [32]. The comparison demonstrates the marginal effects of the vertical component on the rocking response for slender blocks for all practical purposes. On the other hand, some differences are shown for stocky blocks in the uplift neighborhood. Uplift of a rigid block can be a critical condition for a range of (uplift-sensitive) structures or equipment such as liquid-storage tanks, objects of art, computer servers etc. Hence, we proceed with a further investigation of the uplift neighborhood offering a link between the uplift threshold and the ratio of the vertical over the horizontal peak ground acceleration (*PGA*) that can convey the influence of neglecting the vertical acceleration for uplift-sensitive blocks.

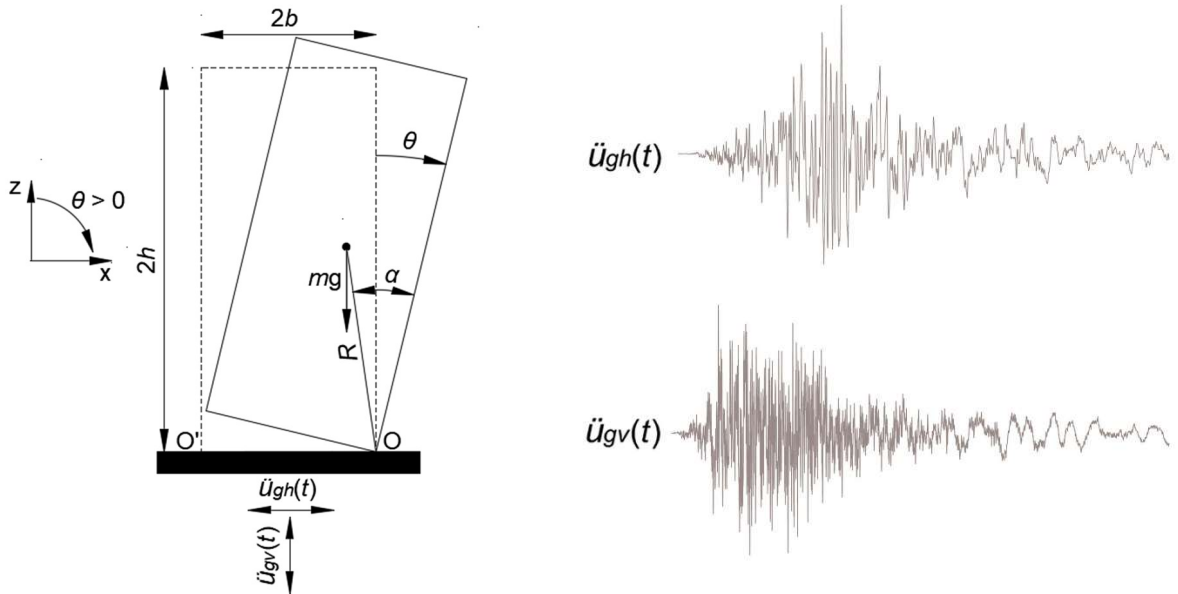## 2 ROCKING RESPONSE OF FREE-STANDING RIGID BLOCKS UNDER HORIZONTAL AND VERTICAL GROUND MOTIONS

Figure 1 presents the planar two-dimensional (2D) rectangular rocking block, having base width of *2b,* height of *2h*, and a uniformly distributed mass *m*. Equivalently, the geometry of the block can be defined by its semi-diagonal *R* and its slenderness angle *α* (Figure 1). The block stands freely on a rigid supporting base and it is subjected to ground excitation. Assuming that the coefficient of friction between the block and its support is high enough to prevent sliding, the seismic response mechanism is pure rocking when the ground shaking is strong enough to trigger uplift. After uplift, the block rocks between its pivot points O-O'. The rocking equation of motion under horizontal excitation has been proposed by Housner [1] and, for a rectangular block, can be expressed in a compact form as [10]:

$$\ddot{\theta} = -p^2 \left[\sin(\alpha \mathrm{sgn}(\theta) - \theta) + \frac{\ddot{u}_{gh}}{\mathrm{g}} \cos(\alpha \mathrm{sgn}(\theta) - \theta) \right] \tag{1}$$

where θ is the tilt (rocking) angle (Figure 1) and $p = \sqrt{(3\mathrm{g})/(4R)}$ is the frequency parameter of the rocking block. The oscillation frequency of a rigid block under free vibration is not constant because it strongly depends on the vibration amplitude [1]. Nevertheless, p is a measure of the dynamic characteristics of the block and is equal to the in-plane pendulum frequency of the block as if it were hanging from its rocking rotation point [33].

Yim et al. [2] have extended the equation of rocking motion to include the vertical component, while Makris and Kampas [26] have expressed it in compact form as:

$$\ddot{\theta} = -p^2 \left[\left(1 + \frac{\ddot{u}_{gv}}{\mathrm{g}}\right) \sin(\alpha \mathrm{sgn}(\theta) - \theta) + \frac{\ddot{u}_{gh}}{\mathrm{g}} \cos(\alpha \mathrm{sgn}(\theta) - \theta) \right] \tag{2}$$

Figure 1 Planar model of a rocking block on a rigid base (left). Horizontal (N-S component), $\ddot{u}_{gh}(t)$, and vertical, $\ddot{u}_{gv}(t)$, excitation recorded in the 1989 Loma Prieta earthquake, Agnews State Hospital station (right).

Energy is only dissipated at impacts (i.e. when the pivot point changes). Housner [1] assumed that the impacts are instantaneous and that the impact forces are concentrated at the new pivot point. Under these assumptions, conservation of angular momentum can be applied to determine the ratio of the post-impact to the pre-impact angular velocity ("Coefficient of Restitution") [9]:

$$\eta = \frac{\dot{\theta}_{after}}{\dot{\theta}_{before}} = 1 - \frac{3}{2}\sin^2\alpha \tag{3}$$

Under purely horizontal ground excitation the block uplifts and starts rocking between its pivot points when the overturning moment due to the seismic excitation exceeds the restoring moment of gravity for the first time. Hence, uplift first occurs when [e.g., 6, 10]:

$$\ddot{u}_{gh} > g\tan\alpha \tag{4}$$

where $\ddot{u}_{gh}$ is the horizontal acceleration and g is the acceleration of gravity. When the vertical component is taken into account, the corresponding condition for block uplift becomes [26]:

$$\ddot{u}_{gh} > \left(1 + \frac{\ddot{u}_{gv}}{g}\right)g\tan\alpha \tag{5}$$

where $\ddot{u}_{gv}$ is the concurrent value of the vertical acceleration.

Even though there can theoretically be cases where the rocking angle θ dynamically exceeds the slenderness angle α without the block overturning, such cases are rare and conservatively, in this paper, we assume that $\theta = \alpha$ results in overturning. Also, in Figure 1, the horizontal and the vertical components are presented for an example ground motion. As shown, the waveform of the vertical component is of higher frequency than that of the horizontal one. The intensity of the vertical component may be higher than the corresponding horizontal component(s) in the near field, yet the vertical over horizontal *PGA* ratio is generally considered to be lower than 1.0 as it tends to attenuate with distance from the rupture [34, 35] especially for events with moment magnitude $M > 5.0$ [36].

3   MODELING AND ANALYSIS

In this section, the geometric and dynamic characteristics of the rigid blocks that are employed as well as the analysis choices for the calculation of their seismic response, with or without including the vertical component, are presented.

3.1 Rocking blocks under investigation

The geometric and the dynamic characteristics of the blocks under investigation are captured in Table 1. Seven different block cases are employed representing blocks of various shapes and sizes. Some of them resemble existing structures whereas the rest are meant to create a range of realistic blocks of differing slenderness and size. Specifically, Block C represents a 2D analogue of a monolithic freestanding ancient column of the Temple of Aphaia in Aegina [17], Greece; Block E resembles a column of the Temple of Athene Nike in Athens [26], whereas Block G is a 2D model of a 32U server cabinet rack, i.e., a cabinet that can fit 32 standard rack units, each of 1.75in or 4.445cm of internal clear height. The four other blocks are arbitrary cases of slender (i.e., A, B) or less slender (i.e., D, F) blocks. Additionally, in Table 1 the values of the coefficient of restitution via Eq. (3) are presented. As shown, by using the α-dependent Eq. (3), the stocky blocks (e.g., G) show considerably higher amount of total energy loss per impact (33%) in comparison with the slender blocks (e.g., 2% energy loss per impact for Block A).

**Table 1.** Geometric and dynamic characteristics of the blocks under investigation.

Block	2*b* (m)	2*h* (m)	α (rad)	*R* (m)	*p* (s^{-1})	η
A	1.50	15.00	0.0997	7.5374	0.9880	0.99
B	1.33	12.00	0.1104	6.0367	1.1040	0.98
C	0.95	5.29	0.1777	2.6873	1.6546	0.95
D	1.00	4.00	0.2450	2.0616	1.8892	0.91
E	0.50	4.00	0.1244	2.0156	1.9106	0.98
F	0.50	2.50	0.1974	1.2748	2.4024	0.94
G	0.60	1.62	0.3547	0.8638	2.9185	0.82

3.2 Multi-stripe Analysis

MSA is employed for determining the seismic response of the rocking blocks. It is applied by running sets of ground motions that have been scaled to match given values of the intensity measure (IM) corresponding to predefined hazard levels, the results appearing in characteristic "stripes" when plotted in IM versus engineering demand parameter (EDP) coordinates. The main advantage of MSA over its main "opponent" Incremental Dynamic Analysis (IDA) [37, 38] is that it can be directly linked with the site-specific seismic hazard via record selection. Record selection [29–31, 39–41] allows selecting ground motions that are consistent with the seismic hazard of a specific site. Herein, we employ records that have been selected by Kohrangi et. al 2020 [31] for the site of Elefsina, Greece. As conditioning IM, the geometric mean (or geomean) of the spectral acceleration of the two horizontal components for a vibration period of 0.3s and 5% viscous damping, $S_{ahgm}(0.3s)$, was employed. Based on the findings of Lin et. al [29], in general, mild changes to the conditioning period do not break hazard consistency. Hence, since the IMs that are used herein are the PGA and the peak ground velocity (PGV), a period of 0.3s is considered to be good enough to maintain some hazard consistency both at short (PGA) and moderate (PGV) periods; this allows us to make record-by-record investigations without needing to reselect records for each IM. Given 7 different hazard levels, which refer to IM values with a return period of 10 to 5000 years, the conditional target spectra were created for both the horizontal (geomean) and the vertical components, fully taking into account the correlation of spectral accelerations at different periods and between the vertical and horizontal component. Thus, at each level 77 natural ground motions were selected from the PEER database [42, 43] to match both the vertical and horizontal conditional spectra, using the so-called CS-Compatible approach [31]. The CS-compatible approach [31] accounts for all relevant correlations between the horizontal and the vertical component of motion when selecting records resulting into selected sets that are hazard consistent both in the horizontal and in the vertical direction. All the selected ground motions were recorded on firm soil whereas they are mainly ordinary (i.e., no pulse-like, no long-duration) records. Some records characterized as pulse-like [44] are included into selection, mainly into the high IM levels, but since in all levels they are less than 10% of the total sample they do not affect the calculations one way or another.

Since $S_{ahgm}(0.3s)$ is not a commonly used IM for rocking blocks, a shift to classic "rocking IMs" [e.g., 45, 46, 47] is of interest. To preserve as much as possible the desirable hazard consistency of CS selected sets, the records in each stripe were (separately) rescaled to match the median value of (i) the geomean peak ground acceleration (PGA_{hgm}) and (ii) the geomean peak ground velocity (PGV_{hgm}) of the horizontal components of the records selected at each of 7 levels of $S_{ahgm}(0.3s)$. For example, Figures 2a-b show the range of PGA_{hgm} and PGV_{hgm} corresponding to the 4th level of $S_{ahgm}(0.3s)$ and the location of the median value in each IM case, 0.61g and 37.84cm/s, respectively. By rescaling each of the 77 records in the stripe to match these new IM levels and running the response history analyses, four sets of MSA results were created, two for PGA_{hgm} (Figure 2c) and two for PGV_{hgm} (Figure 2d) with and without including the vertical component. Both the vertical and the horizontal components were scaled by the same factors in all cases. Given the 2D nature of the model, a single arbitrary horizontal component from each pair was assigned to all blocks. For the analysis under the selected and scaled ground motions, the scripts of Vassiliou [48, 49] for the rocking response of a planar rectangular rigid block were used. These Matlab [50] scripts, solve the rocking equation of motion using the ode45 [50] differential equation solver either under horizontal excitation via Eq. (1) [48], or under both horizontal and vertical excitation via Eq. (2) [49]. The peak absolute rocking angle, θ_{max}, normalized by the block slenderness α was used as the EDP: $\tilde{\theta} = \theta_{max}/\alpha$.

Of the two IMs employed herein, PGA_{hgm} is considered as efficient and sufficient only in the rocking uplift range ($\tilde{\theta} < 0.10$), whereas PGV_{hgm} reigns supreme for higher rocking angles up to and including overturning [47]. Note that the two IMs can be employed in their geomean component form, PGA_{hgm} and PGV_{hgm}, or in their "arbitrary" form, using the values computed for the single horizontal component assigned to the 2D rocking block. Using the geomean values stems from the conventional use of an IM as the interface variable that links the structural response with the seismic hazard [47, 51, 52]. The hazard is typically estimated via ground motion prediction equations [e.g., 53] that refer to the geomean; thus, vulnerability studies are typically conducted on the basis of geomean IM values as well. However, the arbitrary component IMs tend to display somewhat lower dispersions when considering a pure 2D problem, as it is natural that using the IMs characterizing the actual component applied will increase the predictive capability. Still, given the overall high dispersion associated with rocking, this phenomenon mainly manifests itself in the uplift (or rocking initiation) neighborhood, where the PGA_h of the actual horizontal component a "perfect" IM, as it can be directly associated with the rocking initiation in the planar rocking model at $PGA_h \cong g\tan\alpha$. On the other hand, for the PGA_{hgm}, there is some moderate uncertainty in estimating the threshold for rocking uplift due to the different peak values recorded in the two components. This will in turn force us to provide different approaches, one per IM type used.
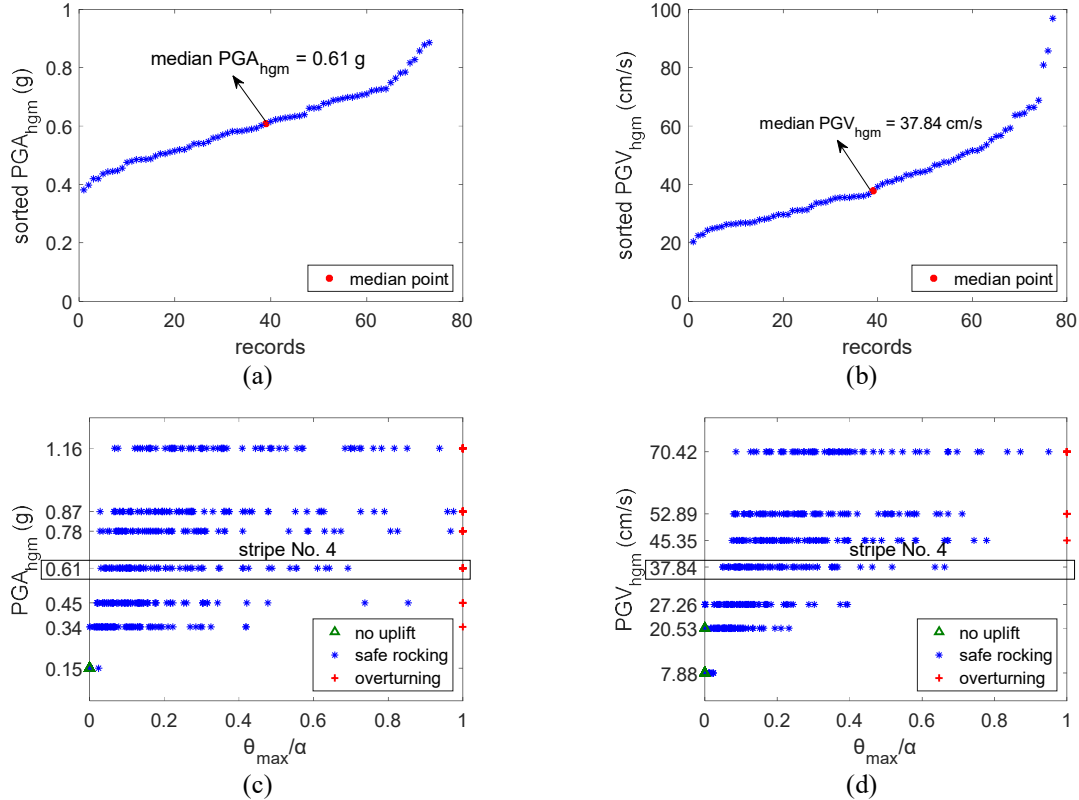
Figure 2. Example of IM conversion from S_{ahgm}(0.3s) to PGA_{hgm} and PGV_{hgm} for the 4th IM level: (a) sorted values of PGA_{hgm} corresponding to the 4th level of S_{ahgm}(0.3s); (b) sorted values of PGV_{hgm} corresponding to the 4th level of S_{ahgm}(0.3s). Example MSA results for Block C without the vertical component, showing how the rescaled records form stripes at the median (c) PGA_{hgm} and (d) PGV_{hgm} values.

4   COMPARISON OF THE ROCKING RESPONSE WITH AND WITHOUT THE VERTICAL COMPONENT

The comparison of the rocking response with and without the vertical component is presented in this section. The comparison starts from the differences that are captured in the response between the two cases on a single ground motion basis and then escalates to the response statistics from the MSA results.

4.1 Comparison on a single ground motion basis

The first step of comparison refers to directly comparing the seismic response under a single ground motion with and without the inclusion of the corresponding vertical component. Figure 3 captures the $\tilde{\theta}$ values for 3 ordinary ground motions of the total sample of 77 for a specific PGV_{hgm} level (i.e., stripe No. 4, PGV_{hgm} = 37.84 cm/s) with and without the vertical component for Block C. As shown, no uniform conclusion can be deduced from the results. The inclusion of the vertical component may lead to detrimental or beneficial impact on the response, while the magnitude of the effect itself can range from considerable (e.g., ground motion 1) to marginal (e.g., ground motion 2, ground motion 3). For instance, for ground motions 1 and 3, the vertical component increases the seismic demand values, either significantly for the former or marginally for the latter. Contrarily, for ground motion 2, including the vertical component leads to lower demand values. These observations can be attributed to the highly nonlinear nature of rocking that is strongly dependent on the waveform of the ground motion and the correlation between vertical and horizontal waveforms when the former is also included into analysis. Thus, a single record case has little to say about the actual influence of the vertical component on the response. Notably, the first ones to suggest that the rocking problem should be treated statistically were Yim et al. [2] as early as 1980, when they reported that "the rocking response of a block is very sensitive to small changes in its size and slenderness ratio and to the details of the ground motion" and that to observe systematic trends one needs to study the problem probabilistically.
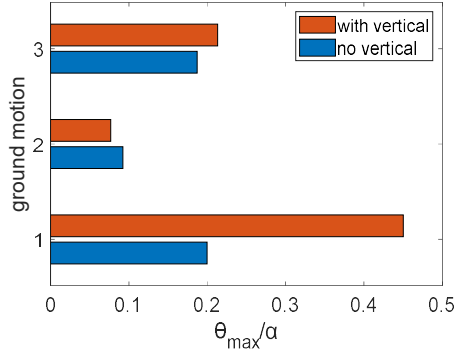
Figure 3. $\tilde{\theta}$ values for 3 of the 77 ground motions in stripe No. 4 of PGV_{hgm} with and without including the vertical component in the analysis of Block C.

4.2 Comparison on an ensemble of ground motions basis

As the comparison on a single record basis has little to offer under high uncertainty, two different approaches for ensemble-level comparisons are employed to determine the influence of the vertical component. First is a paired record-by-record comparison, whereby we take advantage of analysis results under the same horizontal component with and without the vertical. The second is a comparison of statistics characterizing stripes at the same IM level when including versus neglecting the vertical acceleration, comparing central values, dispersions, fragilities, and entire sample distributions. The first approach is considered a stronger test, as it can more reliably detect deviations in the two versions of the problem even when using small samples, in the same way that medical studies can employ a small number of twins to test the effectiveness of a treatment. The second is less sensitive, akin to larger random sample medicinal tests in "similar groups of patients"; still, it is more characteristic of how the results would translate to response distributions and then to performance estimates in practical applications.

For the record-by-record comparison, we turn to the MSA results obtained with and without including the vertical component. For each data point, characterized by the triplet of block, record and IM level, we are first interested in the "matching" of behavior regime between the two sets (i.e., with and without the vertical component) of responses. In other words, we are interested in whether in both cases the system has displayed (i) no uplift ($\tilde{\theta} = 0$), (ii) safe rocking ($0 < \tilde{\theta} < 1$), or (iii) overturning ($\tilde{\theta} \geq 1$). Data points with matching behaviors of no uplift or overturning are considered to constitute a case of non-existent influence of the vertical component. Non-matching cases indicate exactly the opposite. As shown in Figure 4, the matched safe rocking cases are the majority in most of the blocks and IM-levels except for the low IM-levels in the less slender blocks where many matching no-uplifts are observed. This happens due to the direct association of the slenderness angle with the PGA_h required for uplift. For instance, only matched no rocking cases are captured for the Block G in the lower intensity levels since in these levels none of the 77 records is strong enough to trigger rocking for this stocky block. On the other hand, in higher IM-levels some few matched cases of overturning are captured. At worst, only 10% of the ground motions at any stripe show non-matching behavior, as indicated by the 90% to 100% cumulative percentage of matching cases in Figure 4.

6
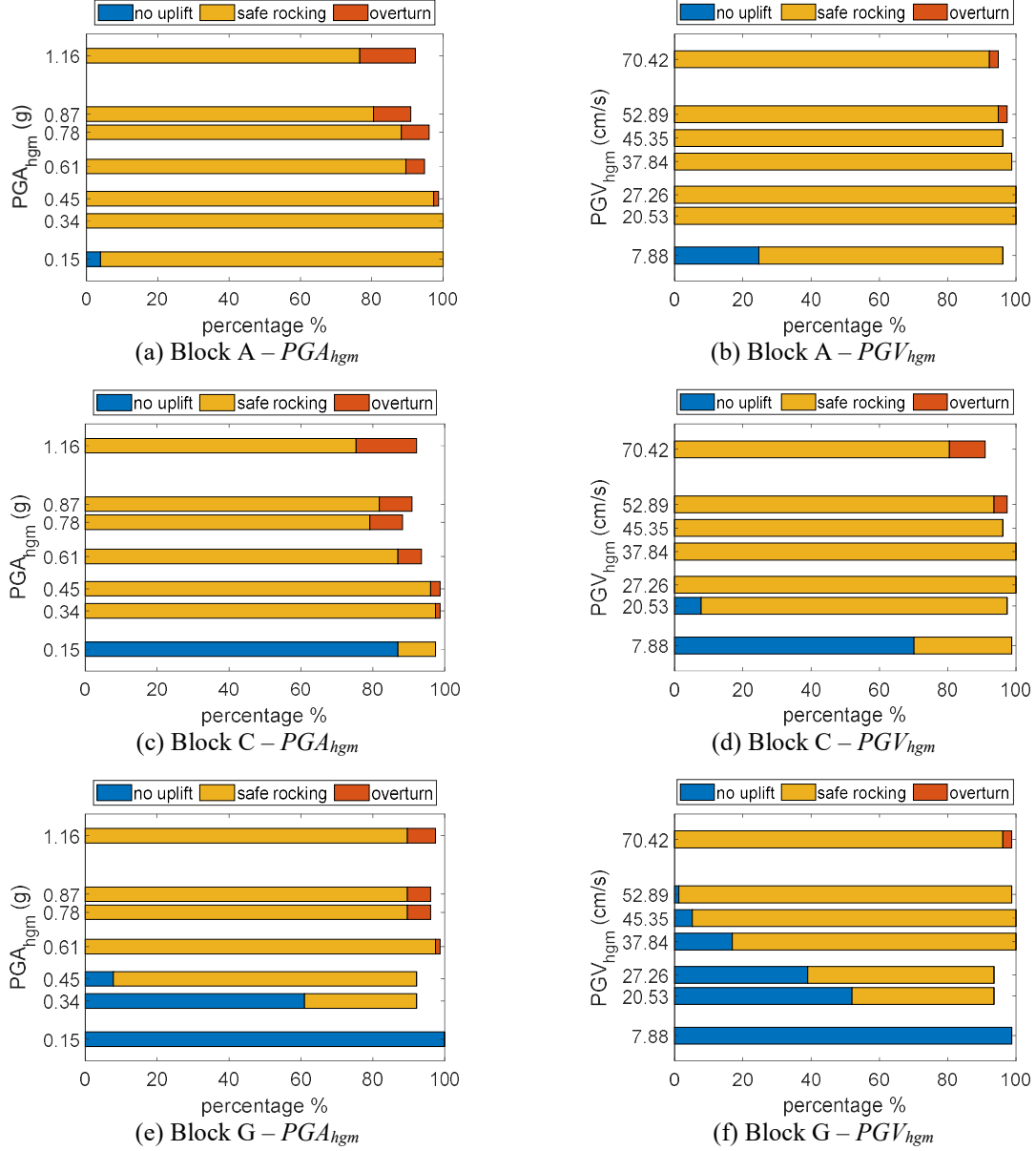
Figure 4. Percentage of records displaying matching behavior of no uplift, safe rocking, or overturning when applied with versus without the vertical component. Blocks A, C, G, using PGA_{hgm} (left) and PGV_{hgm} (right) as IMs.

For cases falling in the safe rocking regime, the ratio of response is needed to further distinguish the existence or not of an effect. Specifically, by taking the full MSA results of the N matching safe rocking per stripe the ratio of the $\tilde{\theta}$ values with and without including the vertical component is computed for the i-th stripe ($i = 1 \dots 7$) and the j-th record ($j = 1 \dots N$) as:

$$r_{v/nv}^{i,j} = \frac{\tilde{\theta}_v^{i,j}}{\tilde{\theta}_{nv}^{i,j}} \tag{6}$$

where $\tilde{\theta}_v^{i,j}$ is the $\tilde{\theta}$ value for the record j in stripe i where both the vertical and the horizontal components are considered, and $\tilde{\theta}_{nv}^{i,j}$ is the corresponding result when only the arbitrary horizontal component is employed. The resulting ratios are presented as boxplots [54] in Figure 5 for four blocks of Table 1. In each horizontal stripe (IM-level) the central mark denotes the median ratio; the notches indicate the 95% confidence interval of the median; the left and right edges of the box denote the 25% and 75% values, respectively; the whiskers the interquartile range. Herein, it was set equal to 1.5 times the 25-75% range. Crosses indicate ratios falling outside the whiskers, which are treated as outliers or extreme values.

7
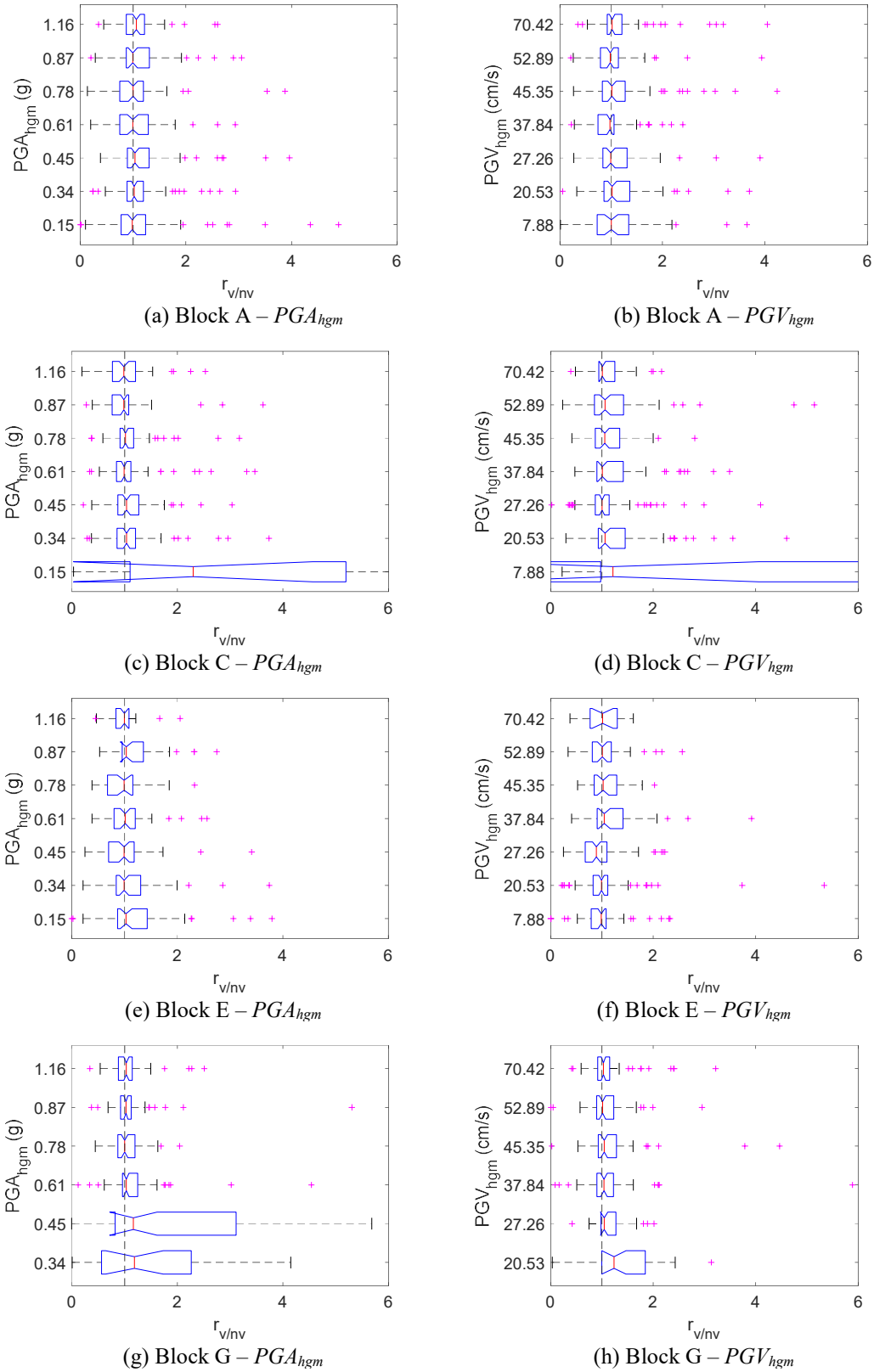
Figure 5. Boxplots of the ratio of response with the vertical component over without, shown for matching safe-rocking cases for Blocks A, C, E, G using PGA_{hgm} (left) and PGV_{hgm} (right) as IMs.
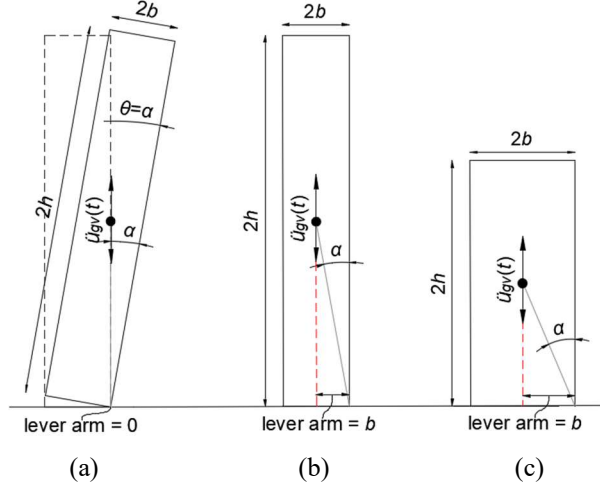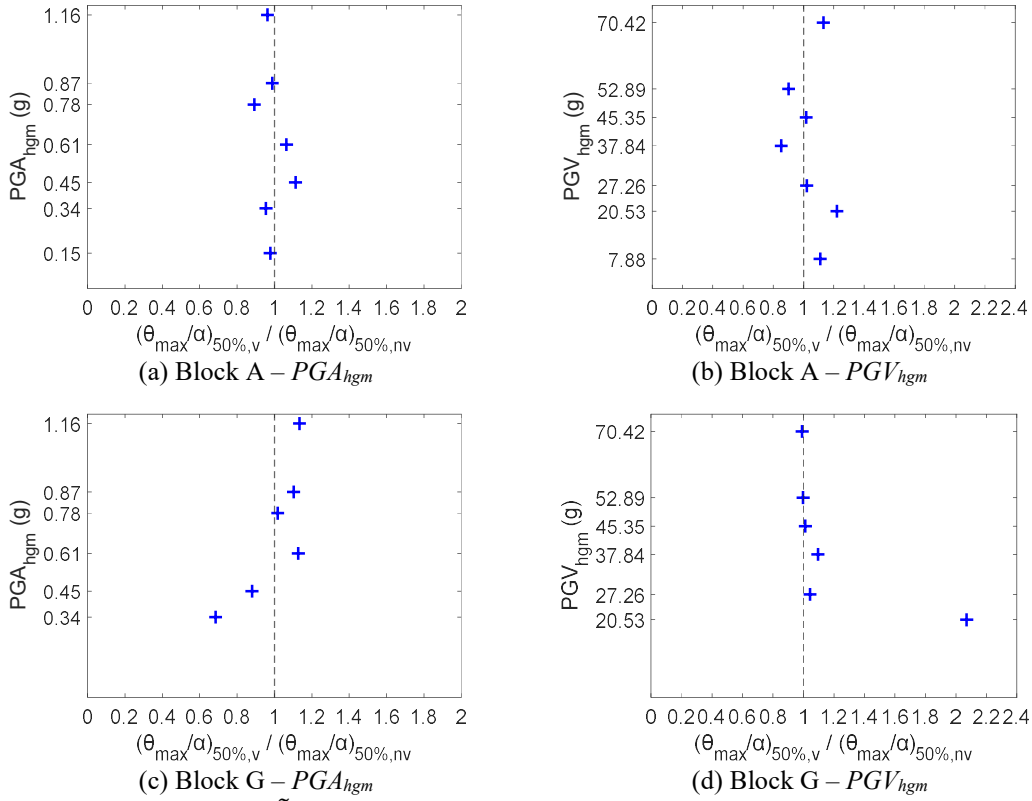
Figure 6. Moment-arm of the vertical component in rocking blocks: (a) slender block near overturning; (b) slender block in rocking initiation; (c) stocky block in rocking initiation.

In general, for the slender blocks (A, B, E) the 95% confidence interval on the median ratio brackets 1 for all the stripes both for PGA_{hgm} and PGV_{hgm}; thus, little influence of the vertical is indicated. When looking at less slender blocks (C, F, D, G) the same observation holds for the higher stripes, away from uplift. On the other hand, no uniform conclusion can be stated for the effect of the vertical component in the rocking initiation neighborhood. For instance, for the stocky Block G the median ratio noticeably differs from 1 when PGV_{hgm} is employed as IM whereas for PGA_{hgm} it remains close to 1 in all cases. Hence, a potential effect cannot be overruled for rocking initiation. There is also a fairly large dispersion of results in the uplift neighborhood, which can be associated with the lower number (i.e., small sample) of matching safe-rocking cases as presented in Figure 4.

Overall, these observations agree with existing literature findings [e.g., 3, 25–27] that block geometry defines the influence of the vertical component. The vertical acceleration is multiplied by $\sin(\alpha\,\text{sgn}(\theta) - \theta)$ in Eq. (2), while the horizontal acceleration by $\cos(\alpha\,\text{sgn}(\theta) - \theta)$. Close to overturning ($\theta \cong \alpha$), the influence of the vertical component is minimal, as $\sin 0 = 0$, or equivalently by virtue of the moment-arm of the vertical component essentially being zeroed out at the precipice of falling over (Figure 6a). On the contrary, the lever arm is maximal (equal to b, Figure 6b) at the verge of uplift ($\theta \cong 0$). Thus, while a relatively low $\alpha < 0.25$ rad (slender blocks) would still result in a low influence of the vertical component, for higher values of α (stockier blocks Figure 6c) the sine and cosine multipliers come closer for $\theta \cong 0$, allowing the observed influence of the vertical acceleration.

Now, we turn to the ensemble statistics of response. Adopting a lognormal distribution assumption [47], we are primarily interested in the median and the standard deviation of the natural logarithm of the response, or $\tilde{\theta}_{50}$ and β, respectively. Obviously only the matching safe rocking responses are considered, as zero or "infinite" overturning responses can play havoc with numerical comparisons. Figure 7 and Figure 8 show the ratio of the resulting $\tilde{\theta}_{50}$ and β values with and without the vertical component per stripe for two representative blocks: slender Block A and stocky Block G. As shown, for both quantities the differences are moderate in most of the cases (less than 20%), with the exception of few levels where differences up to 40% are observed. There is also a large deviant ratio of medians exceeding 2.0 in Figure 7d; this appears for stocky Block G in the lowest PGV_{hgm} stripe implying a non-negligible detrimental effect of the vertical acceleration in the rocking uplift area. Otherwise, there is little evidence to support the existence of significant influence when considering "horizontal" (given IM) sample statistics.

Next, we proceed to the comparison of fragilities. This is directly equivalent to considering "vertical" (given EDP) sample statistics [32], and while it may seem like a superfluous way of reconfirming our findings from horizontal statistics, it carries one important advantage: All three regimes of response can now be treated in a single test (at least when looking at EDP thresholds other than uplift or overturning). Specifically, by taking the full MSA results with and without the inclusion of the vertical component, empirical cumulative distribution functions (CDFs) are calculated for three $\tilde{\theta}$ thresholds representing rocking uplift ($\tilde{\theta} \cong 0$), an intermediate safe rocking condition ($\tilde{\theta} \cong 0.35$), and finally the overturning threshold ($\tilde{\theta} \cong 1.00$). As Figure 9 shows, minor differences appear for both the slender Block A and the stocky Block G. The impact may randomly be beneficial or detrimental, without any clear trend. The only potential exception once again appears in the uplift neighborhood, where the inclusion of the vertical component leads to marginally worse fragilities.

Figure 7. Ratio of the median ($\tilde{\theta}_{50}$) values per stripe for matched safe-rocking cases with (v) and without (nv) including the vertical components into analysis for Blocks A and G.
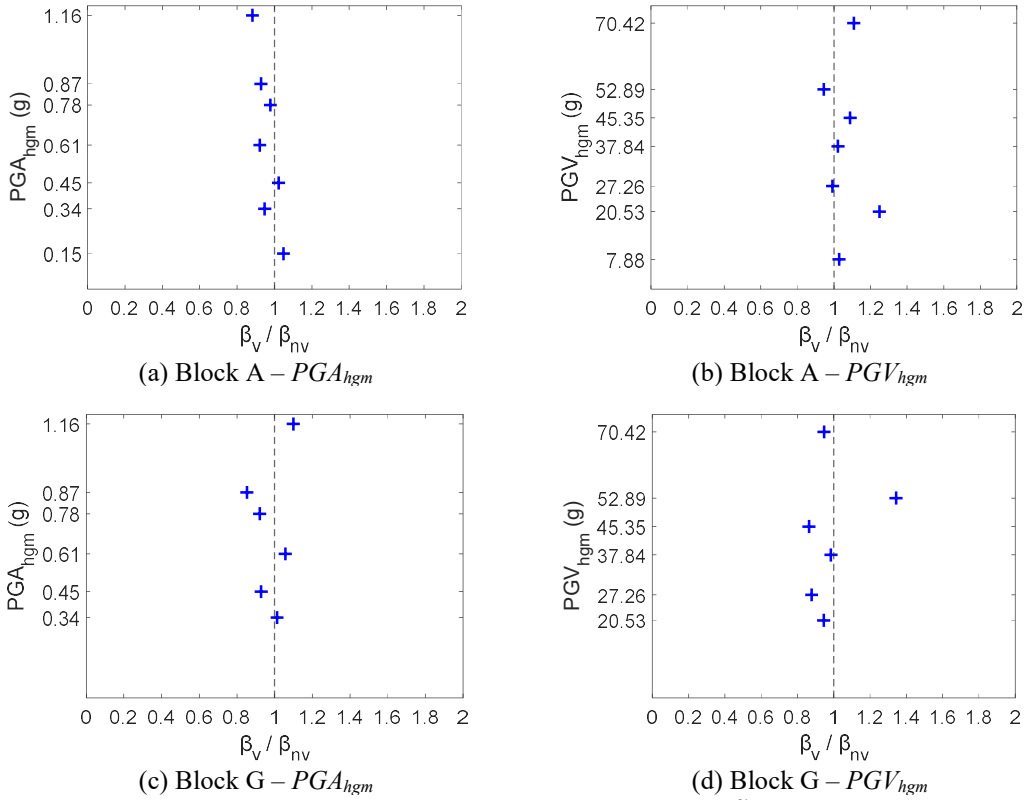

Figure 8. Ratio of the standard deviation of the natural logarithm of the $\tilde{\theta}$ values per stripe for matched safe-rocking cases with (v) and without (nv) including the vertical components into analysis for Blocks A and G.

10
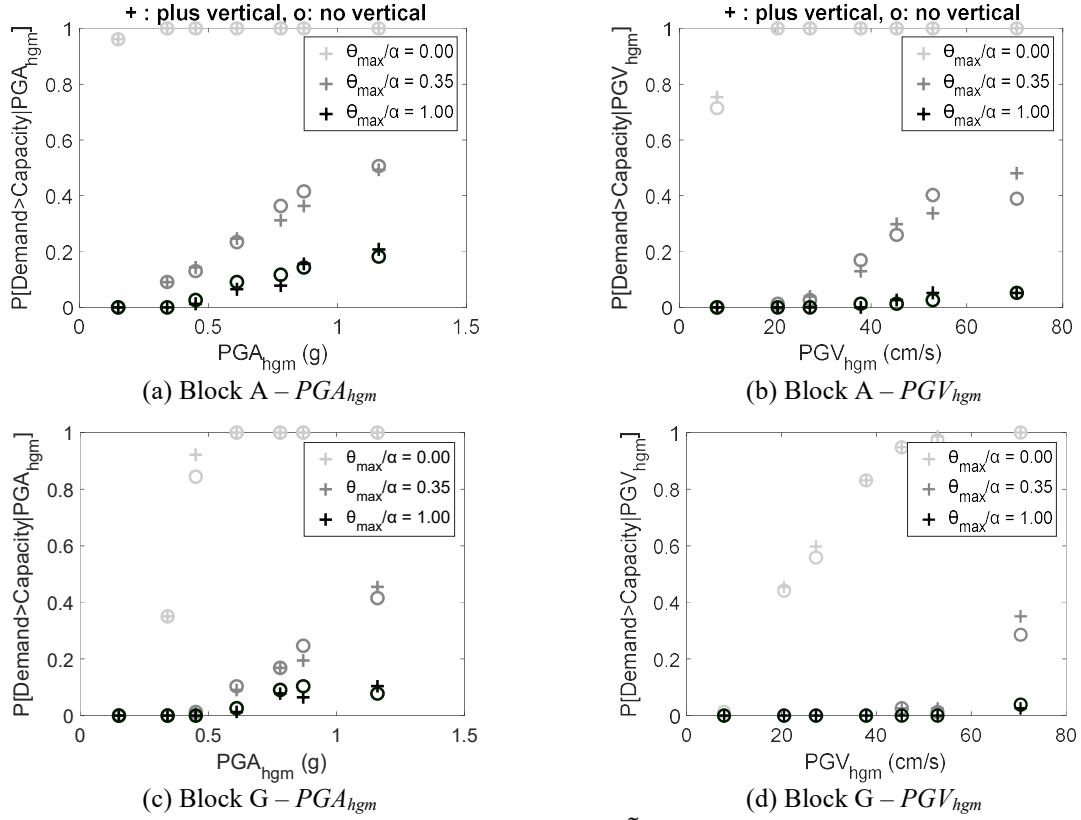
Figure 9. Empirical CDF fragility points at three pre-defined $\tilde{\theta}$ capacity thresholds for given PGA_{hgm} and PGV_{hgm} for two case-study blocks. Estimates with (+) and without (o) the vertical component are compared.

Although the differences appearing in Figure 9 are not visually considerable, proper statistical testing is warranted. For this we employ the two-sample Kolmogorov-Smirnov test [55–57] at each stripe to formally compare the distribution of samples with and without the vertical component. This statistical test checks the null hypothesis that the two tested samples come from the same continuous distribution. All the 77 values of $\tilde{\theta}$ are considered, regardless of the rocking regime where they fall in. To avoid superfluous responses, all overturning cases were assigned a value of $\tilde{\theta} = 1.00$. Figure 10 illustrates an example of the test p-values obtained for Blocks A and G. p-values higher than 0.05 are found at all stripes, thus we do not have enough evidence to reject the null hypothesis at the 95% significance level. In other words, there is little support that the vertical component has any significant influence, at least not that can be reliably detected when 77 records are employed. These observations stand for all seven blocks and both IMs employed, showing that even the moderate differences captured in Figures 7–9 are not statistically significant.

(a) Block A – PGA_{hgm} (b) Block A – PGV_{hgm}

(c) Block G – PGA_{hgm} (d) Block G – PGV_{hgm}
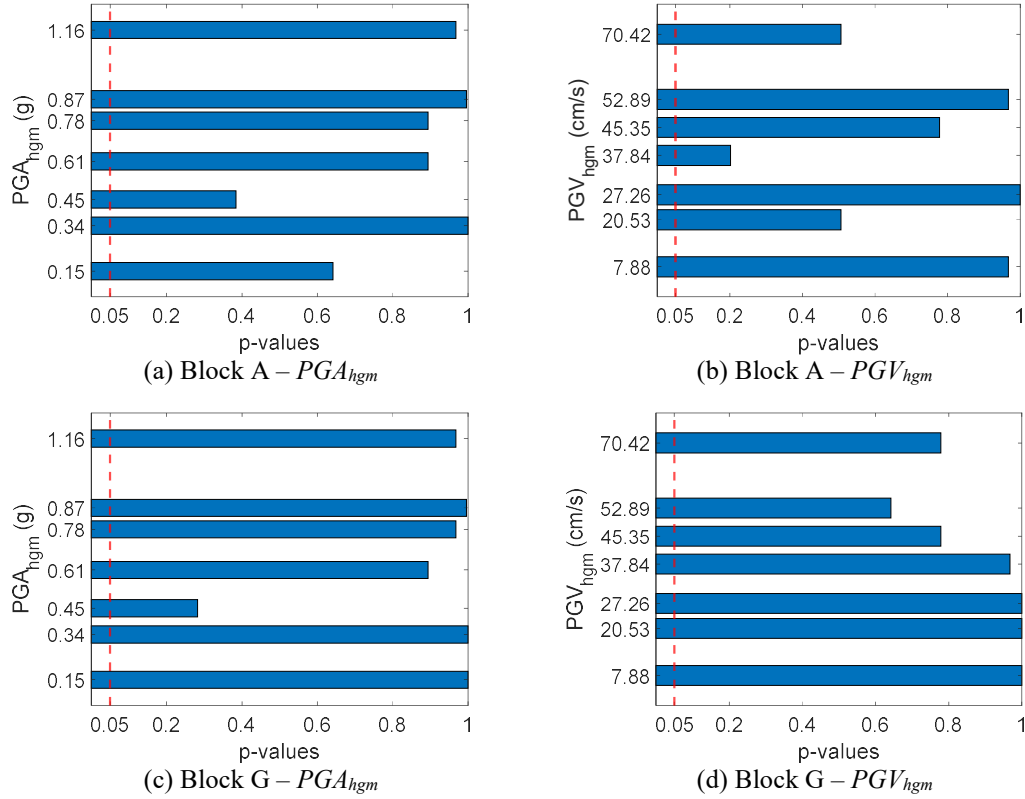
Figure 10. *p*-values of the two-sample Kolmogorov Smirnov test estimated at each stripe when comparing the samples of $\tilde{\theta}$ with and without the vertical component for Blocks A and G.

5   INFLUENCE OF THE VERTICAL COMPONENT IN THE ROCKING INITIATION AREA

Although the effect of the vertical component on the rocking response seems to be marginal in most of the previous comparison stages, as discussed earlier, it may still influence rocking uplift for stocky blocks. Even in such cases, though, the influence of the vertical acceleration rapidly fades away as one moves away from the uplift region. In practice, accounting for this effect makes sense only for cases where even a small uplift is associated with damage, as is the case with, e.g., overall brittle objects (such as objects of art), edges/toes vulnerable to crushing, or unanchored liquid storage tanks prone to elephant foot buckling. Quantifying this effect at the initiation of rocking can provide a practical upper bound to the influence of vertical acceleration in this range of response. Since the effect mainly appears for the stockier of the blocks of Table 1 some extra stocky blocks are added at this stage with the characteristics appearing in Table 2. These additional blocks have slenderness angles ranging within 0.44-0.67 rad. The upper value of 0.67 rad refers to a very stocky block that may be more prone to sliding rather than rocking. However, we assume that the supporting surface's coefficient of friction is high enough to assure the pure rocking response.

Table 2. Geometric and dynamic characteristics of the extra stocky blocks.

| Block	2*b* (m)	2*h* (m)	*α* (rad)	*R* (m)	*p* (s⁻¹)	*η*
H	2.40	5.00	0.4475	2.7731	1.6289	0.72
I	0.60	1.00	0.5404	0.5831	3.5522	0.60
J	3.00	4.00	0.6435	2.500	1.7155	0.46
K	0.80	1.00	0.6747	0.6403	3.3898	0.41
L	1.60	2.00	0.6747	1.2806	2.3969	0.41

For the analysis, the full set of blocks in Tables 1 and 2 undergo an iterative analysis procedure. Specifically, by taking the 77 records (both the horizontal and the vertical component) of the lowest MSA stripe of the previous section that correspond to the low-hazard area, a new block-specific set of stripes is created in the neighborhood

of uplift for different ratios of vertical versus horizontal PGA. Multiple ratios are considered for both the arbitrary horizontal component, as PGA_v/PGA_h, and the geomean one, or PGA_v/PGA_{hgm}. In both cases, the new set of stripes is employed for the twelve blocks (A to L) by scaling per record the horizontal component to nine IM levels ranging from 0.60 to 1.20 times the uplift threshold of $g\tan\alpha$, given six different ratios of vertical versus horizontal PGA varying within 0 (i.e., analysis only with the horizontal component) and 1.25 (i.e., the vertical component is scaled to be 1.25 times the corresponding horizontal component). This may preserve hazard consistency in the horizontal direction, but it probably breaks it in the vertical. Still, given that it is only the effect of the peak accelerations that is investigated under near-static conditions, this is a loss of no consequence. It is also important here to say that for high levels of vertical acceleration the block may eventually jump, completely losing contact with the supporting surface [27]. Such bouncing of the block cannot be captured by our simplified model; this could be an issue if one is interested in fully characterizing the block behavior, yet it is not problematic in our case as such an excitation will surely force uplift of the simplified model. In other words, the appearance of damage will not be mischaracterized.

For each block and vertical/horizontal ratio, after employing MSA for the new sets of stripes by using the scripts of Vasilliou [48-49], the uplift ($\tilde{\theta} > 0$) empirical fragility CDF is calculated; then a lognormal distribution is fitted via the maximum likelihood approach [58] as presented in Figures 11–12. In all cases, the vertical component mainly affects the stocky blocks by reducing the median IM to trigger uplift. The effect is attenuated as the blocks become more slender (lower α). Regarding the two different IMs employed, for the case of PGA_h, zero dispersion is captured in the fragilities for the no vertical case since the uplift is directly associated with the PGA_h of the arbitrary component. Contrarily, for the PGA_{hgm}, a constant dispersion approximately equal to 0.17 is captured for the no vertical uplift fragilities in all the block cases. This dispersion stems from the differences in intensity between the two horizontal components of each pair and it is essentially a property of the record set used, rather than the block itself; actually, a similar dispersion has been found using a different record set in [59]. One more observation worth mentioning is that, for both IMs the uplift fragilities of two blocks of same slenderness and different sizes (i.e., Block K and Block L) are almost identical (results of Block K are not shown herein for reasons of brevity). This observation stems from the fact that the investigation considers only the uplift region, which is strongly associated only with the block's slenderness angle α. For higher levels of response, larger differences between the two blocks are expected, since additional parameters, i.e., block size and ground motion characteristics beyond PGA, will affect the response of each block.

13

(a) Block A

(b) Block C

(c) Block G

(d) Block H

(e) Block I

(f) Block L
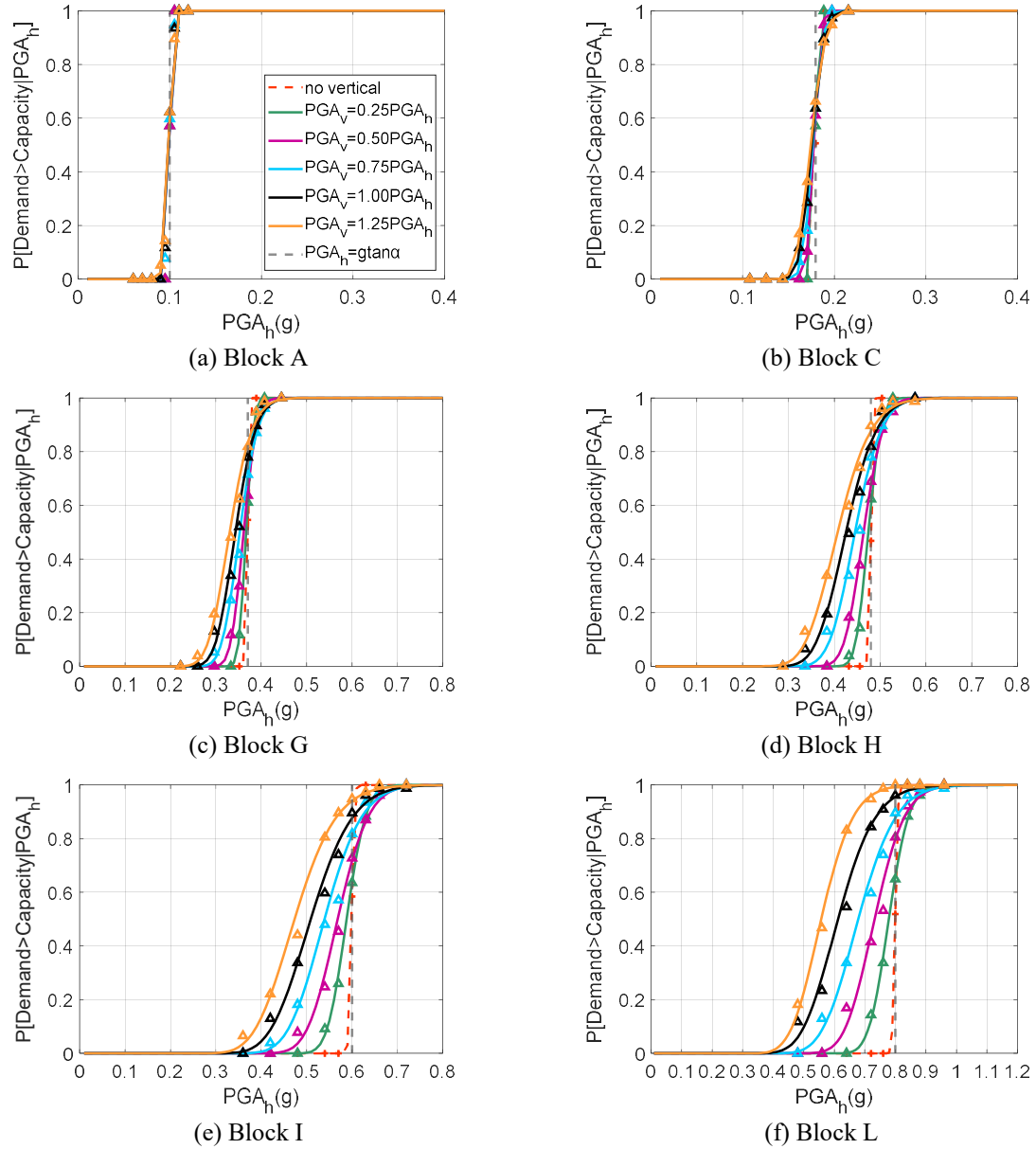
Figure 11. Fragility functions (empirical CDF points plus lognormal fit) for rocking uplift (i.e., $\tilde{\theta} > 0$) given the arbitrary component PGA_h for different ratios of PGA_v / PGA_h .
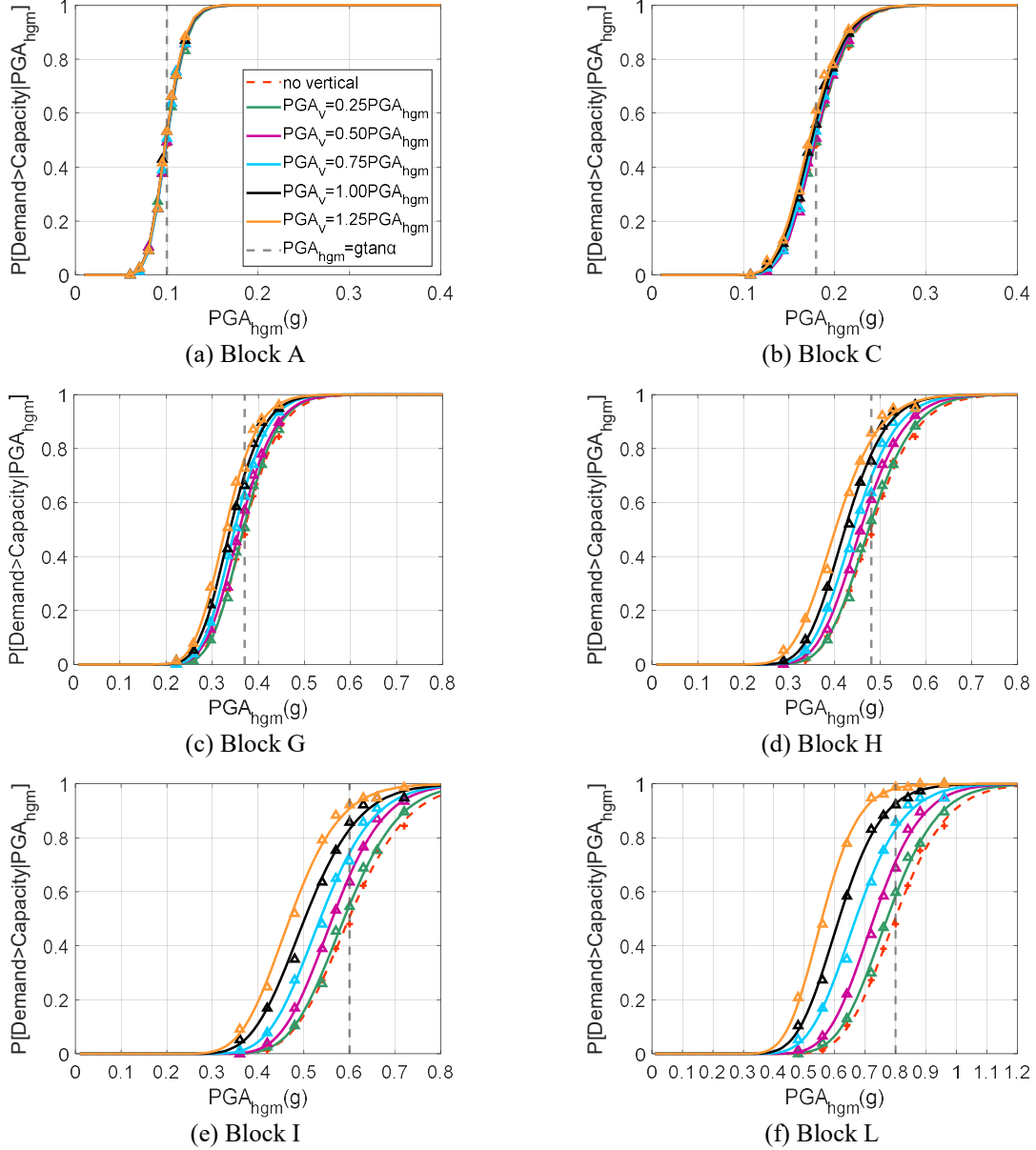
Figure 12. Fragility functions (empirical CDF points plus lognormal fit) for rocking uplift (i.e., $\tilde{\theta} > 0$) given the geomean component PGA_{hgm} for different ratios of PGA_v / PGA_{hgm}.

Since the lognormal distribution model shows excellent promise in fitting the uplift fragilities, we seek trends in its two defining parameters: the median IM (PGA_{h50}, or PGA_{hgm50}), here taken minus the rocking uplift threshold of Eq. (4), disregarding the vertical component for simplicity, and the dispersion (β_h, or β_{hgm}). This shifting (or reduction) of the median IM by $g \tan \alpha$ allows us to efficiently zoom into the effect of the vertical acceleration, as we take out the (larger) main effect of the horizontal. Specifically, for the case of PGA_h, both median and dispersion follow a linear pattern with respect to PGA_v / PGA_h (Figure 13a-b). Hence, a linear regression in the form of $y = b_1 x$ is found to be an efficient fit for both ($PGA_{h50} - g \tan \alpha$) and β_h against PGA_v / PGA_h, showing high R^2 values, as shown in Figure 13a-b. The slope of the lines shows that the effect of the vertical component is higher for the stocky blocks (i.e., Block L). On the other hand, for the case of PGA_{hgm}, different trends are found to fit ($PGA_{hgm5} - g \tan \alpha$) and β_{hgm} against PGA_v / PGA_{hgm}. For the former, a classic linear model in the form of $y = b_1 x + b_2$ is a good choice (Figure 13c), whereas for the latter a constant dispersion of about 0.17 is accurate enough for all blocks (Figure 13d). As illustrated in Figure 13a classic linear model with a constant term may be more appropriate for some block cases (e.g. Block L) also for the case of ($PGA_{h50} - g \tan \alpha$). However, since under PGA_h the uplift threshold under only the horizontal component (i.e., $PGA_v / PGA_h = 0$) is deterministically defined, a linear regression model without a constant term is preferred for this case. In addition, differences between the two models are expected to be minor, whereas the adopted model seems to fit efficiently the majority of the blocks employed. In all cases, the results for Block K replicate Block L since they share the same slenderness

angle; thus Block K is removed from all subsequent fitting to achieve a homogenous sample rather than placing double weight on one specific value of α.
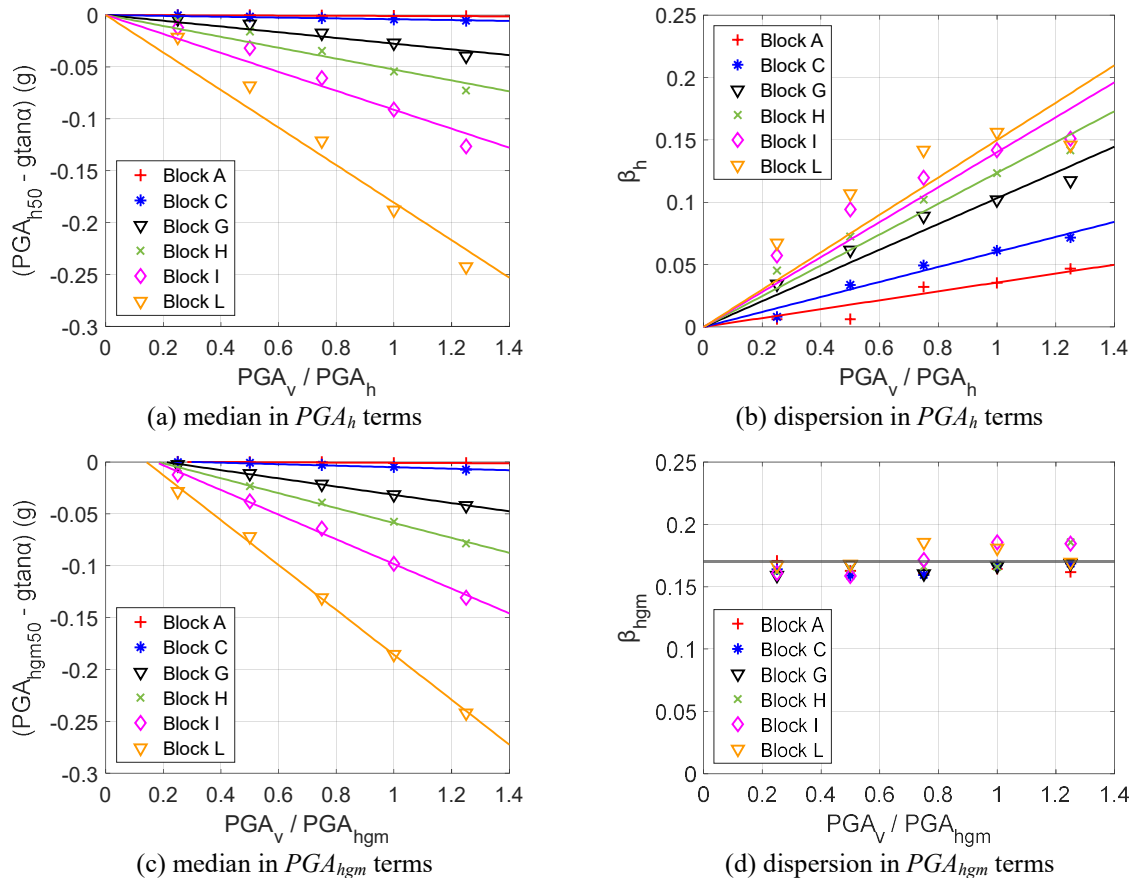

Figure 13. Linear regression of IM median and dispersion for the rocking initiation of six of the blocks under investigation against: (a)-(b) the ratio PGA_v / PGA_h; (c)-(d) the ratio PGA_v / PGA_{hgm}.
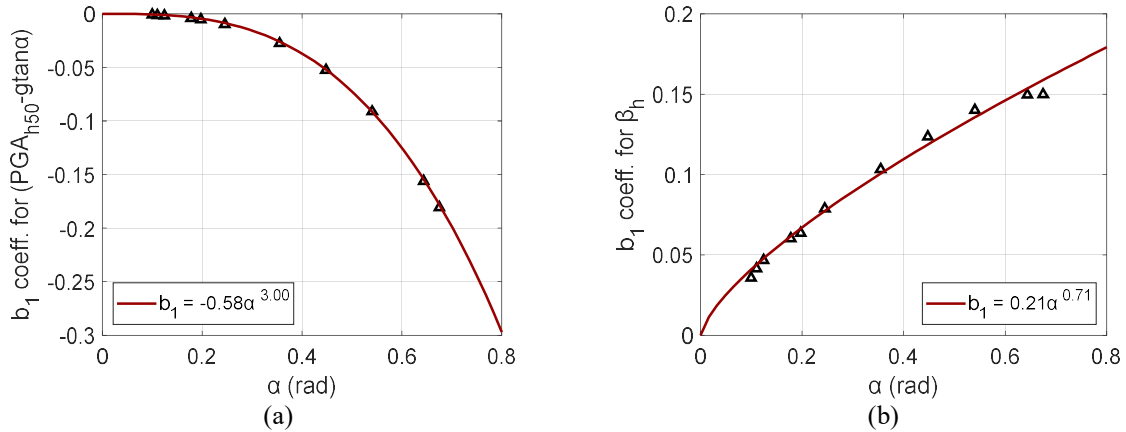
Figure 14. Power-law fit to the b_1 coefficients used for capturing $(PGA_{h50} - g \tan \alpha)$ and β_h versus the blocks' slenderness angle α.

In a second regression step, the coefficients estimated for the IM median and dispersion are correlated with the slenderness angle α. For PGA_h, again, a fitting without intercept is desired for both quantities; for $\alpha \to 0$, per the geometric interpretation of Figure 6, there should be a near-zero influence of the vertical component in the uplift neighborhood, thus b_1 should tend to zero. From the data points in Figure 14, a power-law offers a good fit for both the median and the dispersion's b_1 coefficients. Following a similar pattern for the case of PGA_{hgm}, a power-law fit is also found efficient for fitting b_1 and b_2 for $(PGA_{hgm50} - g \tan \alpha)$ as shown in Figure 15.

16
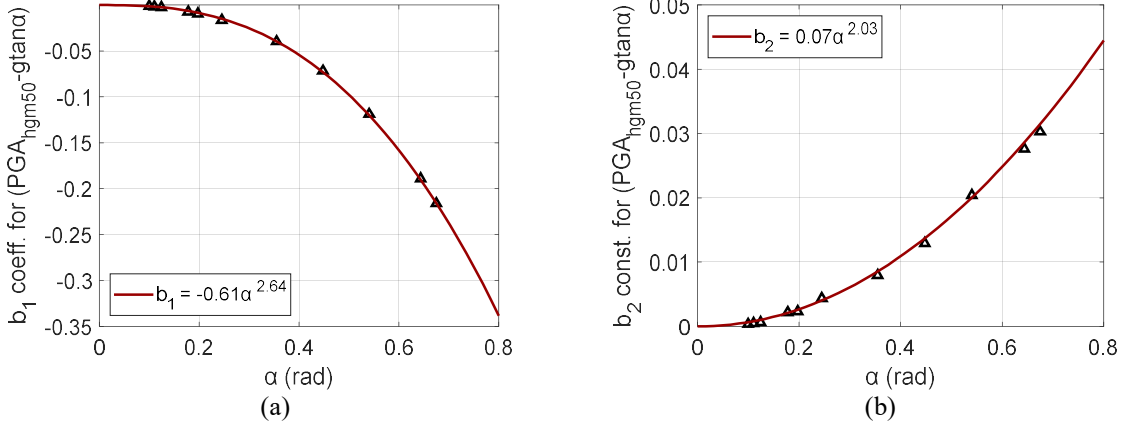
Figure 15. Power-law fit to the b_1 and b_2 coefficients used to capture $(PGA_{hgm50} - g\tan\alpha)$ versus the blocks' slenderness angle α.

After this two-level fitting procedure, the median estimates of $(PGA_{h50} - g\tan\alpha)$ and β_h used to define the lognormal fragility of rocking uplift can be expressed as a function of two parameters, namely α in rad and PGA_v / PGA_h, as:

$$\frac{(PGA_{h50} - g\tan\alpha)_{50}}{g} = -0.58\alpha^{3.00}\left(\frac{PGA_v}{PGA_h}\right) \tag{7}$$

$$\beta_{h50} = 0.21\alpha^{0.71}\left(\frac{PGA_v}{PGA_h}\right) \tag{8}$$

In retrospect, the expressions employed for Eq. (7), (8) are amenable to a single stage linear regression in logarithmic space that would allow the direct determination of all coefficients as well as the associated standard error. In other words, such a regression would conform to a lognormal model of the output, which is why we named the results as median estimates, rather than means. Either way, for the total $k = 55$ non-zero points comprising eleven values of α times five vertical/horizontal ratio levels, the model dispersion around the medians of Eqs (7), (8) can be calculated as:

$$\sigma_{lny} = \frac{1}{k-2}\sqrt{\sum_{i=1}^{k}(\ln y_i - \ln y_i')^2} \tag{9}$$

where y_i refers to the $k = 55$ median (minus $g\tan\alpha$) or dispersion values resulting from the block fragilities, while the y_i' are the corresponding predictions of Eqs (7), (8). The resulting error dispersions via Eq. (9) are 0.0649 for the median $(PGA_{h50} - g\tan\alpha)_{50}$ and 0.0447 for the dispersion β_{h50}. Given the lognormality assumption, both values can be interpreted as coefficients of variation of 6.5% and 4.5%, respectively, and are practically insignificant, indicating a good fit.

For the case of PGA_{hgm} the fitted expressions are:

$$\frac{(PGA_{hgm50} - g\tan\alpha)_{50}}{g} = \min\left\{-0.61\alpha^{2.64}\left(\frac{PGA_v}{PGA_{hgm}}\right) + 0.07\alpha^{2.03}, \quad 0\right\} \tag{10}$$

$$\beta_{hgm50} = 0.17 \tag{11}$$

For the central value, we chose to employ a hard cut-off value at zero, discarding any minor exceedances (seemingly increases of the median) at low PGA_v / PGA_{hgm}. Overall, the forms of Eq. (10), (11) do not clearly support lognormality, necessitating a closer look at the residuals. Still, expecting a similarly good fit and to avoid overcomplicating the situation, lognormality was adopted and the standard errors via Eq. (9) are 0.1041 for the median $(PGA_{hgm5} - g\tan\alpha)_{50}$ and 0.0068 for the dispersion (β_{hgm50}). Once again, the errors are minimal; therefore, whether we chose or not the proper distribution model for the residuals is of little consequence.

Now, as a simple example of practical application, the case of server racks is considered. These are uplift-sensitive components since they contain hard drives with specific acceleration tolerances; any impact due to uplift may cause a head crash, potentially resulting to complete loss of the hard drive [60]. Three racks of the same 0.60m base width are considered: a 15U rack with a total height of 0.87m (α= 0.60 rad), a 20U rack of 1.09 m (α= 0.50 rad), a 30U of 1.53 m (α= 0.37 rad), and a 42U of 2.05 m (α= 0.28 rad). The (median) parameters of the lognormal uplift fragility estimated via Eq. (7)–(8) for the arbitrary component are presented in Figure 16. As expected, when the vertical acceleration is neglected (i.e PGA_v /PGA_h = 0) the central value becomes PGA_h = gtanα, whereas the dispersion β_{h50} is equal to 0. When the ratio of the vertical-to-horizontal acceleration increases, as would be the case for sites closer to a fault, the median uplift threshold universally shifts to lower PGA_h values. This reduction can range from noticeable, for the stockier 15U or 20U racks, to marginal for the less stocky 42U rack. At the same time, the dispersion is increased. Overall, the 15U server loses ~20% of its median capacity when the peak vertical acceleration equals the horizontal, with higher ratios proportionally reducing the uplift threshold. This loss drops to ~10% for the 20U rack and becomes much less pronounced for the taller 30U and 42U. Whether these values carry any appreciable consequences for the seismic safety of such sensitive equipment is beyond the scope of our study. For what it is worth, this is the effect of the vertical acceleration on the uplift safety of simple rigid blocks and Eqs (7)–(8) and (10)–(11) capture it to near perfection.
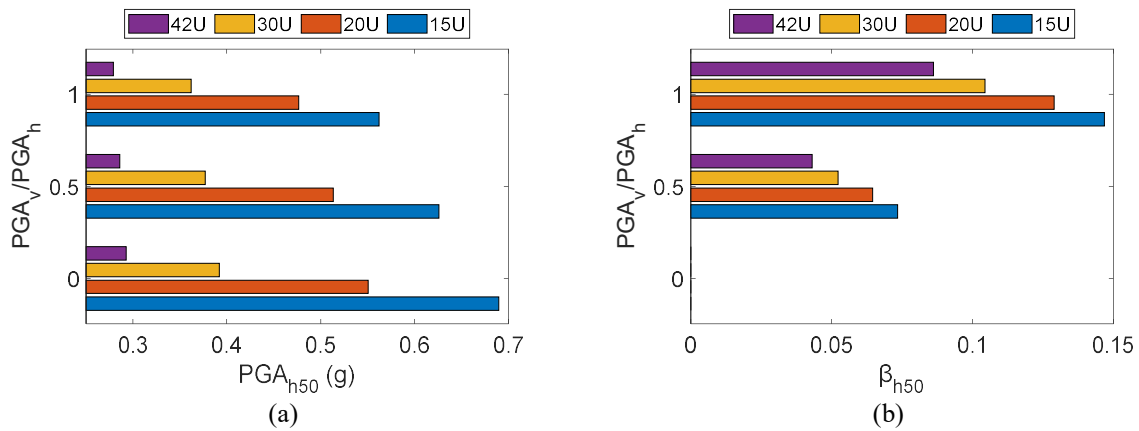
Figure 16. Example of using Eqs (7), (8) to assess (a) the median and (b) the dispersion of the lognormal uplift fragility function of four server racks, 15/20/30/42U, listed from stockier to more slender.

6   CONCLUSIONS

A detailed investigation has been presented on the impact of including the vertical component of the seismic excitation into the analysis of rocking blocks under a probabilistic view. After investigating thoroughly the seismic response of multiple rigid blocks varying in shape and size, the main findings can be summarized as follows:

➢ On a single-ground-motion basis, the differences in the response when the vertical component is included can vary from moderate to considerable between different records whereas the vertical component may arbitrarily lead to higher or lower seismic demands for the block. This can be attributed to the nature of the rocking problem that is highly sensitive to small changes in its parameters.

➢ On a sample-of-records basis, the impact of the vertical component is found to be marginal for the slender blocks or even for the stocky ones for all practical purposes of moderate to large rocking response and overturning. Therefore, one can conclude that neglecting the vertical component does not induce any bias in the probability of reaching or exceeding response values in these regimes. However, the vertical component may influence the uplift of stocky blocks due to the geometry of the problem: For large slenderness angles and when the block is about to start rocking, the vertical component appears in the equation of motion multiplied by a factor of similar magnitude to the factor multiplying the horizontal component. This last observation stems from the geometry of the problem and is in accordance with existing literature.

➢ A higher peak vertical ground acceleration linearly reduces the horizontal acceleration needed to cause uplift. The median and the dispersion of a lognormal uplift fragility can be reliably predicted from the slenderness angle (α) and the vertical over horizontal peak ground acceleration ratio.

18

Finally, a comprehensive approach is offered for probabilistically investigating the influence of different modeling parameters, loading conditions and system properties on seismic demand and capacity; it may have only been showcased for simple rocking blocks, but can be employed with practically any other structural system.

ACKNOWLEDGEMENTS

DATA AVAILABILITY STATEMENT

The data that support the findings of this study are available from the corresponding author upon reasonable request.

CONFLICT OF INTEREST STATEMENT

The authors declare that they have no conflicts of interest.

REFERENCES

[1] Housner GW. The behavior of inverted pendulum structures during earthquakes. *Bulletin of the Seismological Society of America*, 1963;**53**(2):403–417.

[2] Yim C-S, Chopra AK, Penzien J. Rocking response of rigid blocks to earthquakes. *Earthquake Engineering and Structural Dynamics*, 1980;**8**(6):565–587. https://doi.org/10.1002/eqe.4290080606

[3] Ishiyama Y. Motions of rigid bodies and criteria for overturning by earthquake excitations. *Earthquake Engineering and Structural Dynamics*, 1982;**10**(5):635–650. https://doi.org/10.1002/eqe.4290100502

[4] Spanos PD, Koh AS. Rocking of Rigid blocks due to harmonic shaking. *Journal of Engineering Mechanics (ASCE)*, 1984;**110**(11):1627–1642. https://doi.org/10.1061/(ASCE)0733-9399(1984)110:11(1627)

[5] Makris N, Roussos Y. Rocking response of rigid blocks under near-source ground motions. *Géotechnique*, 2000;**50**(3):243–262.

[6] Zhang J, Makris N. Rocking response of free-standing blocks under cycloidal pulses. *Journal of Engineering Mechanics (ASCE)*, 2001;**127**(5):473–483. https://doi.org/10.1061/(ASCE)0733-9399(2001)127:5(473)

[7] Makris N, Konstantinidis D. The rocking spectrum and the limitations of practical design methodologies. *Earthquake Engineering and Structural Dynamics*, 2003;**32**(2):265–289. https://doi.org/10.1002/eqe.223

[8] Vassiliou MF, Makris N. Analysis of the rocking response of rigid blocks standing free on a seismically isolated base. *Earthquake Engineering and Structural Dynamics*, 2012;**41**(2):177–196. https://doi.org/10.1002/eqe.1124

[9] Dimitrakopoulos EG, DeJong MJ. Revisiting the rocking block: closed-form solutions and similarity laws. *Proceedings of the Royal Society A: Mathematical, Physical and Engineering Sciences*, 2012;**468**(2144):2294–2318. https://doi.org/10.1098/rspa.2012.0026

[10] Makris N, Vassiliou MF. Planar rocking response and stability analysis of an array of free-standing columns capped with a freely supported rigid beam. *Earthquake Engineering and Structural Dynamics*, 2013;**42**(3):431–449. https://doi.org/10.1002/eqe.2222

[11] Dimitrakopoulos EG, Fung EDW. Closed-form rocking overturning conditions for a family of pulse ground motions. *Proceedings of the Royal Society A: Mathematical, Physical and Engineering Sciences*, 2016;**472**(2196):20160662. https://doi.org/10.1098/rspa.2016.0662

[12] Bachmann JA, Vassiliou MF, Stojadinović B. Dynamics of rocking podium structures. *Earthquake Engineering and Structural Dynamics*, 2017;**46**: 2499–2517. https://doi.org/10.1002/eqe.2915

[13] Bachmann JA, Strand M, Vassiliou MF, Broccardo M, Stojadinović B. Is rocking motion predictable? *Earthquake Engineering and Structural Dynamics*, 2018;**47**(2):535–552. https://doi.org/10.1002/eqe.2978

[14] DeJong MJ. Seismic response of stone masonry spires: analytical modeling. *Engineering Structures*, 2012;40:556–565**.** https://doi.org/10.1016/j.engstruct.2012.03.010

[15] Kalliontzis D, Schultz AE. Characterizing the in-plane rocking response of masonry walls with unbonded posttensioning. *Journal of Structural Engineering (ASCE)*, 2017;**143**(9):04017110. https://doi.org/10.1061/(ASCE)ST.1943-541X.0001838

[16] Papantonopoulos C, Psycharis IN, Papastamatiou DY, Lemos JV, Mouzakis HP. Numerical prediction of the earthquake response of classical columns using the distinct element method. *Earthquake Engineering and Structural Dynamics*, 2002;**31**(9):1699–1717. https://doi.org/10.1002/eqe.185

[17] Melissianos VE, Lachanas CG, Vamvatsikos D. Preliminary Seismic Risk Assessment of Monolithic Columns of the Aphaia Temple in Aegina. *In: Vayas I., Mazzolani F.M. (eds) Protection of Historical Constructions. PROHITECH 2021. Lecture Notes in Civil Engineering*, 2022:209. Springer, Cham. https://doi.org/10.1007/978-3-030-90788-4_48

[18] Thonstad T, Mantawy IM, Stanton JF, Eberhard MO, Sanders DH. Shaking table performance of a new bridge system with pretensioned rocking columns. *Journal of bridge Engineering (ASCE)*, 2016;**21**(4):04015079. https://doi.org/10.1061/(ASCE)BE.1943-5592.0000867

[19] Xie Y, Zhang J, DesRoches R, Padgett JE. Seismic fragilities of single-column highway bridges with rocking column-footing. *Earthquake Engineering and Structural Dynamics*, 2019;**48**(7):843–864. https://doi.org/10.1002/eqe.3164

[20] Konstantinidis D, Makris, N. Experimental and analytical studies on the response of freestanding laboratory equipment to earthquake shaking. *Earthquake Engineering and Structural Dynamics*, 2009;**38**:827–848. https://doi.org/10.1002/eqe.871

[21] Dar A, Konstantinidis D, El‐Dakhakhni WW. Evaluation of ASCE 43‐05 seismic design criteria for rocking objects in nuclear facilities. *Journal of Structural Engineering (ASCE)*, 2016;**142**(11):04016110. https://doi.org/10.1061/(ASCE)ST.1943-541X.0001581

[22] Dimentberg MF, Lin YK, Zhang R. *Toppling of computer type equipment under base excitation, Journal of Engineering Mechanics (ASCE)* 1993;**119**(1):145–160. https://doi.org/10.1061/(ASCE)0733-9399(1993)119:1(145)

[23] Taniguchi T. Non-linear response analyses of rectangular rigid bodies subjected to horizontal and vertical ground motion. *Earthquake Engineering & Structural Dynamics*, 2002;**31**(8):1481–1500.

[24] Shi B, Anooshehpoor A, Zeng Y, Brune JN. Rocking and overturning of precariously balanced rocks by earthquakes. *Bulletin of the Seismological Society of America*, 1996;**86**(5):1364–1371.

[25] Makris N, Zhang J. Rocking response and overturning of anchored equipment under seismic excitation. Rep. No. PEER 1999-06. Berkeley, CA: Pacific Earthquake Engineering Research Center, Univ. of California, 1999.

[26] Makris N, Kampas G. Size versus slenderness: two competing parameters in the seismic stability of free-standing rocking columns. *Bulletin of the Seismological Society of America*, 2016;**106**(1):104. http://dx.doi.org/10.1785/0120150138

[27] Linde SA, Konstantinidis D, Tait MJ. Rocking response of unanchored building contents considering horizontal and vertical excitation. *Journal of Structural Engineering (ASCE)*, 2020;**146**(9)04020175. https://doi.org/10.1061/(ASCE)ST.1943-541X.0002735

[28] Jalayer F, Cornell CA. Alternative non-linear demand estimation methods for probability-based seismic assessments. *Earthquake Engineering and Structural Dynamics*, 2009;**38**(8):951–972. https://doi.org/10.1002/eqe.876

[29] Lin T, Haselton CB, Baker JW. Conditional spectrum-based ground motion selection. Part I: hazard consistency for risk-based assessments. *Earthquake Engineering and Structural Dynamics* 2013;**42**(12):1847–1865. https://doi.org/10.1002/eqe.2301

[30] Kohrangi M, Bazzurro P, Vamvatsikos D. Conditional spectrum bidirectional record selection for risk assessment of 3D structures using scalar and vector IMs. *Earthquake Engineering & Structural Dynamics*, 2019;**48**(9): 1066–1082. https://doi.org/10.1002/eqe.3177

[31] Kohrangi M, Bazzurro P, Bakalis K, Vamvatsikos D. Bi-directional conditional-spectra-based record selection for horizontal and vertical ground motions. *Proceedings of the 17th World Conference on Earthquake Engineering, 17WCEE*, Sendai, Japan, 2020.

[32] Bakalis K, Vamvatsikos D. Seismic fragility functions via nonlinear response history analysis. *Journal of Structural Engineering (ASCE)*, 2018;**144**(10):04018181. https://doi.org/10.1061/(ASCE)ST.1943-541X.0002141

[33] Dimitrakopoulos EG, DeJong MJ. Overturning of Retrofitted Rocking Structures under Pulse-Type Excitations. *Journal of Engineering Mechanics*. 2012; **138**(8):963–972. https://doi.org/10.1061/(ASCE)EM.1943-7889.0000410

[34] Bozorgnia Y, Campbell KW. The vertical-to-horizontal response spectral ratio and tentative procedures for developing simplified V/H and vertical design spectra. *Journal of Earthquake Engineering*, 2004;**8**(2):175–207. https://doi.org/10.1080/13632460409350486

[35] Bozorgnia Y, Campbell KW. Ground Motion Model for the Vertical-to-Horizontal (V/H) Ratios of PGA, PGV, and Response Spectra. *Earthquake Spectra*, 2016;**32**(2):951–978. https://doi.org/10.1193/100614eqs151m

[36] Akkar S, Sandıkkaya MA, Ay BÖ. Compatible ground-motion prediction equations for damping scaling factors and vertical-to-horizontal spectral amplitude ratios for the broader Europe region. *Bull Earthquake Eng* 2014;**12**:517–547. https://doi.org/10.1007/s10518-013-9537-1

[37] Vamvatsikos D, Cornell CA. Incremental dynamic analysis. *Earthquake Engineering and Structural Dynamics*, 2002;**31**(3):491–514. https://doi.org/10.1002/eqe.141

[38] Lachanas CG, Vamvatsikos D. Rocking incremental dynamic analysis. *Earthquake Engineering and Structural Dynamics*, 2022;**51**(3):688–703. https://doi.org/10.1002/eqe.3586

[39] Baker JW, Cornell CA. Spectral shape, epsilon and record selection. *Earthquake Engineering and Structural Dynamics*, 2006;**35**(9):1077–1095. https://doi.org/10.1002/eqe.571

[40] Bradley BA. A generalized conditional intensity measure approach and holistic ground-motion selection. *Earthquake Engineering and Structural Dynamics*, 2010;**39**(12):1321–1342. https://doi.org/10.1002/eqe.995

[41] Kohrangi M, Vamvatsikos D, Bazzurro P. Multi-level conditional spectrum-based record selection for IDA. *Earthquake Spectra*, 2020;**36**(4):1976–1994. https://doi.org/10.1177/8755293020919425

[42] PEER NGA Database. Pacific Earthquake Engineering Research Center, Berkeley, CA, 2005 http://peer.berkeley.edu/nga/ (February. 7, 2022).

[43] Chiou B, Darragh R, Gregor N, Silva W. NGA Project Strong-Motion Database. *Earthquake Spectra*, 2008;**24**(1):23–44. http://dx.doi.org/10.1193/1.2894831

[44] Shahi SK, Baker JW. An efficient algorithm to identify strong velocity pulses in multi-component ground motions. *Bulletin of the Seismological Society of America.* 2014;**104**(5):2456–2466. http://dx.doi.org/10.1785/0120130191

[45] Makris N, Black CJ. Evaluation of peak ground velocity as a "good" intensity measure for near-source ground motions. *Journal of Engineering Mechanics (ASCE)*, 2004;**130**(9):1032–1044. https://doi.org/10.1061/(ASCE)0733-9399(2004)130:9(1032)

[46] Dimitrakopoulos EG, Paraskeva TS. Dimensionless fragility curves for rocking response to near-fault excitations. *Earthquake Engineering and Structural Dynamics*, 2015;**44**(12):2015–2033. https://doi.org/10.1002/eqe.2571

[47] Lachanas CG. Seismic response standardization and risk assessment of simple rocking bodies: Cultural heritage protection, content losses, and decision support solutions. PhD thesis. National Technical University of Athens. (in progress).

[48] Vassiliou MF. Script for the seismic response of a planar rocking block, MATLAB script: available at http://hdl.handle.net/20.500.11850/521016, http://dx.doi.org/10.3929/ethz-b-000521016 last accessed February 2022.

[49] Vassiliou MF. Script for the seismic response of a planar rocking block under horizontal and vertical excitation, MATLAB script: available at http://hdl.handle.net/20.500.11850/531080, http://dx.doi.org/10.3929/ethz-b-000531080 last accessed February 2022.

[50] Matlab version 2019a, the language of technical computing; 2019.

[51] Baker JW, Cornell CA. Which spectral acceleration are you using? *Earthquake Spectra*. 2006;**22**(2):293-312. https://doi.org/10.1193/1.2191540.

[52] Kazantzi AK, Vamvatsikos D. Intensity measure selection for vulnerability studies of building classes. *Earthquake Engineering & Structural Dynamics*, 2015;**44**(15): 2677–2694. https://doi.org/10.1002/eqe.2603

[53] Boore DM, Atkinson GM. Ground-motion prediction equations for the average horizontal component of PGA, PGV, and 5%-damped PSA at spectral periods between 0.01 s and 10.0 s. *Earthquake Spectra* 2008;**24**(1):99–138. http://dx.doi.org/10.1193/1.2830434

[54] McGill R, Tukey JW, Larsen WA. Variations of boxplots. *The American Statistician*. 1978;**32**(1):12–16.

[55] Massey FJ. The Kolmogorov-Smirnov test for goodness of fit. *Journal of the American Statistical Association,* 1951;**46**(253):68–78.

[56] Miller LH. Table of percentage points of Kolmogorov statistics. *Journal of the American Statistical Association,* 1956;**51**(273):111–121.

[57] Marsaglia G, Tsang W, Wang J. Evaluating Kolmogorov's distribution. *Journal of Statistical Software*, 2003;**8**(18):1–4. https://doi.org/10.18637/jss.v008.i18

[58] Baker JW. Efficient analytical fragility function fitting using dynamic structural analysis. *Earthquake Spectra*. 2015;**31**(1):579–599. https://doi.org/10.1193/021113EQS025M

[59] Kazantzi AK, Lachanas CG, Vamvatsikos D. Seismic response distribution expressions for on-ground rigid rocking blocks under ordinary ground motions. *Earthquake Engineering and Structural Dynamics*, 2021;**50**(12):3311–3331 https://doi.org/10.1002/eqe.3511

[60] Yu Wang, Qiang Miao and M. Pecht, "Health monitoring of hard disk drive based on Mahalanobis distance," *2011 Prognostics and System Health Management Conference*, 2011;1-8 DOI: 10.1109/PHM.2011.5939558